

We are IntechOpen, the world's leading publisher of Open Access books Built by scientists, for scientists

6,900

Open access books available

186,000

International authors and editors

200M

Downloads

Our authors are among the

154

Countries delivered to

TOP 1%

most cited scientists

12.2%

Contributors from top 500 universities



WEB OF SCIENCE™

Selection of our books indexed in the Book Citation Index
in Web of Science™ Core Collection (BKCI)

Interested in publishing with us?
Contact book.department@intechopen.com

Numbers displayed above are based on latest data collected.
For more information visit www.intechopen.com



Leading Edge Receptivity at Subsonic and Moderately Supersonic Mach Numbers

Marvin E. Goldstein and Pierre Ricco

Abstract

This chapter is a review of the receptivity and resulting global instability of boundary layers due to free-stream vortical and acoustic disturbances at subsonic and moderately supersonic Mach numbers. The vortical disturbances produce an unsteady boundary layer flow that develops into oblique instability waves with a viscous triple-deck structure in the downstream region. The acoustic disturbances (which have phase speeds that are small compared to the free stream velocity) produce boundary layer fluctuations that evolve into oblique normal modes downstream of the viscous triple-deck region. Asymptotic methods are used to show that both the vortically and acoustically-generated disturbances ultimately develop into modified Rayleigh modes that can exhibit spatial growth or decay depending on the nature of the receptivity process.

Keywords: boundary layer, boundary layer receptivity, compressible boundary layers, global instability

1. Introduction

This chapter is concerned with the effect of unsteady free-stream disturbances on laminar to turbulent transition in boundary layer flows. The exact mechanism depends on the nature and intensity of the disturbances. Transition at high disturbance levels (say $>1\%$) usually begins with the excitation of low frequency streaks in the boundary layer flow that eventually break down into turbulent spots. This phenomena was initially studied by Dryden [1] and much later for compressible flows by Marensi et al. [2]. But the focus of this chapter is on low free stream disturbances levels (say less than 1%) where the transition usually results from a series of events beginning with the generation of spatially growing instability waves by acoustic and/or vortical disturbances in the free-stream. This so-called receptivity phenomenon results in a boundary value problem and therefore differs from classical instability theory which results in an eigenvalue problem for the Rayleigh or Orr-Sommerfeld equations that only apply when the mean flow can be treated as being nearly parallel (see, for example, Reshotko, [3]). The relevant boundary conditions cannot be imposed on the Orr-Sommerfeld or Rayleigh equations in the infinite Reynolds number limit being considered here but the free-stream disturbances can produce unsteady boundary layer perturbations in regions of rapidly changing mean flow that eventually produce unstable Rayleigh or Orr-Sommerfeld

equation eigensolutions further downstream. These regions of nonparallel flow can result from surface roughness elements [4, 5], blowing or suction effects [6] or from the nonparallel mean flow that occurs near the boundary layer leading edge [7, 8].

The mechanism is similar in all cases but the simplest and arguably the most fundamental of these is the one resulting from the nonparallel leading edge flow and the focus here is, therefore, on that case. The initial studies were carried out for two dimensional incompressible flows. Ref. [7] used a low frequency parameter matched asymptotic expansion to show that there is an overlap domain where appropriate asymptotic solutions to the forced boundary layer equations (which apply near the edge) match onto the so-called Tollmien-Schlichting waves that satisfy the Orr-Sommerfeld equation in a region that lies somewhat further downstream. The coupling to the free-stream disturbances turns out to be fairly weak for the two dimensional incompressible flow considered in [7] due to the relatively large decay of boundary layer disturbances upstream of the Tollmien-Schlichting wave region where the Orr-Sommerfeld equation applies.

But there can be a much stronger coupling in supersonic flows which can support a number of different instabilities [9]. The coupling mechanism can be either viscous or inviscid and the instability can either be of the viscous Tollmien-Schlichting type or can be purely inviscid when the mean boundary layer flow has a generalized inflection point. The inviscid coupling, which was first analyzed in [10], tends to be dominant when the obliqueness angle θ of the disturbance differs from the critical angle, $\theta_c \equiv \cos^{-1}(1/M_\infty)$, where the M_∞ is the free-stream Mach number, by an $O(1)$ amount. **Figure 1** shows that the theoretical results of Ref. [10] are in good agreement with experimental data when $\Delta\theta \equiv \theta_c - \theta = O(1)$ but the agreement breaks down when $\theta \rightarrow \theta_c$ [12] and a new rescaled analysis was carried out in Ref. [11] to deal with this case.

Fedorov and Khokhlov [10] analyzed the generation of inviscid instabilities in a supersonic flat plate boundary layer by fast and slow acoustic disturbances in the free stream. They showed that the slow acoustic mode propagates downstream/upstream when the obliqueness angle θ of the acoustic disturbances is smaller/larger than the critical angle θ_c and that downstream propagating slow acoustic modes with $\Delta\theta > 0$ generate unsteady boundary layer disturbances that match onto the inviscid 1st Mack mode instability without undergoing any significant decay. The

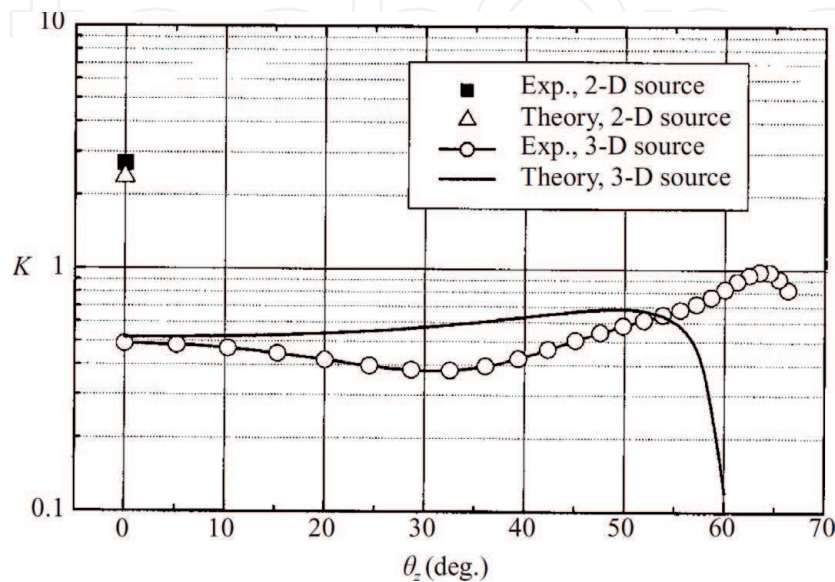


Figure 1.
Comparison of the Fedorov/Khokhlov solution with experiment [12].



Figure 2.
 Low-sweep Aerion AS2 supersonic Bizjet. $M_{\infty} \leq 1.5$. Posted by Tim Brown on the Manufacturer Newsletter.

focus of that reference was on hypersonic flows while the interest here is in the moderately supersonic regime (Mach number less than 4), where the so called 1st Mack mode is the dominant instability, but (as shown in Section 6) emerges much too far downstream to be of practical interest when generated by the inviscid mechanism analyzed in [7]. The instability produced by the small $\Delta\theta$ analysis of Ref. [11] can, however, occur much further upstream when $\Delta\theta$ is sufficiently small. But there is a smallest value of $\Delta\theta$ for which the instability wave coupling can occur.

Smith [13] showed that viscous instabilities, which exhibit the same triple-deck structure as the subsonic Tollmien-Schlichting waves, can also occur at supersonic speeds when the obliqueness angles θ is greater than the critical angle θ_c . Their phase speeds are very small and they must therefore be produced by a viscous wall layer mechanism similar to the one identified in [7].

The analysis of Ref. [7] was extended to compressible subsonic and supersonic flat plate boundary layer flows by Ricco and Wu [14] who showed that highly oblique vortical disturbances can generate a limiting form of the Smith instability [13]. They found that the instability wave lower branch lies further upstream at supersonic speeds than the subsonic lower branch and much further upstream than the incompressible lower branch considered in [7], which means that the instability wave/free-stream disturbance coupling is much greater at supersonic speeds than it is in the incompressible flow considered in [7]. Goldstein and Ricco [11] show that the instability does not possess an upper branch in this case and matches onto a low frequency (short streamwise wavenumber) Rayleigh instability (that can be identified with the 1st Mack mode) when the downstream distance is slightly smaller than the downstream distance where acoustically generated instability corresponding to the smallest possible $\Delta\theta$ emerges. It therefore makes sense to consider both of these receptivity mechanisms simultaneously.

As noted above, the present chapter is concerned with the unsteady flow in a flat plate boundary layer generated by mildly oblique vortical disturbance and small $\Delta\theta$ acoustic disturbances in a moderately supersonic Mach number free stream. The results are expected to be relevant to transition in the straight wing boundary layers on supersonic aircraft such as the low-sweep Aerion AS2 Bizjet, shown in **Figure 2**.

2. Imposed free-stream disturbances

Since the boundary layer is believed to be convectively unstable, the receptivity phenomena are best illustrated by considering a small amplitude harmonic distortion with angular frequency ω^* superimposed on a subsonic or moderately low

Mach number supersonic flow of an ideal gas past an infinitely thin flat plate with uniform free-stream velocity U_∞^* , temperature T_∞^* , dynamic viscosity μ_∞^* and density ρ_∞^* . The velocities, pressure fluctuations, temperature and dynamic viscosity are normalized by U_∞^* , $\rho_\infty^* (U_\infty^*)^2$, T_∞^* and μ_∞^* , respectively. The time t is normalized by ω^* and the Cartesian coordinates, say $\{x, y, z\}$, are normalized by $L^* \equiv U_\infty^* / \omega^*$ with the coordinate y being normal to the plate.

As noted above the phenomenon is analyzed by requiring the Reynolds number $Re = \rho_\infty^* U_\infty^* L^* / \mu_\infty^*$ to be large, or equivalently requiring the frequency parameter $\mathcal{F} \equiv 1/Re$ to be small, and using asymptotic theory to explain how the imposed harmonic distortion generates oblique instabilities at large downstream distances in the viscous boundary layer that forms on the surface of the plate. The natural expansion parameter turns out to be

$$\varepsilon \equiv \mathcal{F}^{1/6}. \quad (1)$$

The free-stream disturbances will be inviscid at the lowest order of approximation and, as is well known [15], can be decomposed into an acoustic component that carries no vorticity, and vortical and entropic components that produce no pressure fluctuations. But only the first two will be considered here.

The vortical disturbance \mathbf{u}_v is given

$$\mathbf{u}_v = \{u_v, v_v, w_v\} = \hat{\delta} \{u_\infty, v_\infty, w_\infty\} \exp[i(x - t + \gamma y + \beta z)], \quad (2)$$

where $\hat{\delta} \ll 1$ is a common scale factor and $u_\infty, v_\infty, w_\infty$ satisfy the continuity condition

$$u_\infty + \gamma v_\infty + \beta w_\infty = 0 \quad (3)$$

but are otherwise arbitrary constants while the acoustic component is governed by the linear wave equation which has a fundamental plane wave solution

$$\{\mathbf{u}_a, p_a\} = \{u_a, v_a, w_a, p_a\} = \frac{\hat{\delta}}{1 - \alpha} \{\alpha, \gamma, \beta, 1 - \alpha\} e^{i(\alpha x + \gamma y + \beta z - t)}, \quad (4)$$

for the velocity and pressure perturbation $\{\mathbf{u}_a, p_a\}$ where

$$\gamma = \sqrt{(M_\infty^2 - 1)(\alpha - \alpha_1)(\alpha - \alpha_2)}, \quad \alpha_{1,2} = \frac{M_\infty^2 \pm \sqrt{M_\infty^2 + \beta^2(M_\infty^2 - 1)}}{M_\infty^2 - 1} \quad (5)$$

and, as noted in Section 1, M_∞ denotes the free-stream Mach number.

The leading edge interaction will produce large scattered fields for $O(1)$ values of the incidence angles $\tan^{-1}(v_a/u_a) = \tan^{-1}(\gamma/\alpha)$ and $\tan^{-1}(v_v/u_v)$ of the acoustic and vortical disturbances, respectively. And, in order to focus on the fundamental mechanisms, we assume that the incidence angles of the vortical disturbances are small and that the incidence angles of the acoustic disturbances are zero, which requires that

$$v_\infty/u_\infty \ll 1 \quad (6)$$

for the former disturbances and that

$$\alpha = \alpha_\mp = M_\infty \cos \theta / (M_\infty \cos \theta \mp 1), \quad \theta \equiv \tan^{-1}(\beta/\alpha), \quad (7)$$

for the latter, where the subscripts $-/+$ refer to the slow/fast acoustic modes. Eq. (7) shows that the slow mode wavenumber becomes infinite when the obliqueness angle is equal to the critical angle referred to in the introduction.

3. Boundary layer disturbances

As indicated above our interest here is in explaining how the incident harmonic distortions generate oblique instabilities at large downstream distances in the viscous boundary layer that forms on the surface of the plate. We begin by considering the fluctuations imposed on this flow by the free-stream vortical disturbance (2).

3.1 Boundary layer disturbances generated by the free-stream vorticity

As noted in the introduction, these disturbances will generate oblique Tollmien-Schlichting instability waves which are known to exhibit a triple-deck structure in the vicinity of their lower branch which lies at an $O(\varepsilon^{-2})$ distance downstream [13] of the leading edge in the high Reynolds number flow being considered here. The Tollmien-Schlichting waves will have $O(\varepsilon^{-1})$ spanwise wavenumbers and we therefore require that

$$\bar{\beta} \equiv \varepsilon\beta = O(1) \quad (8)$$

since the spanwise wavenumber must remain constant as the disturbances propagate downstream.

The continuity condition (3) and the obliqueness restriction (6) will be satisfied if we put

$$\bar{w}_\infty \equiv w_\infty/\varepsilon = O(1), \quad \bar{v}_\infty \equiv v_\infty/\varepsilon = O(1), \quad \bar{\gamma} \equiv \varepsilon\gamma = O(1). \quad (9)$$

The vortical velocity (2) will then interact with the plate to produce an inviscid velocity field [12] that generates a slip velocity at the surface of the plate which must be brought to zero in a thin viscous boundary layer whose temperature, density and streamwise velocity, say $T(\eta)$, $\rho(\eta)$, $U(\eta)$, respectively, are assumed to be functions of the Dorodnitsyn-Howarth variable

$$\eta \equiv \frac{1}{\varepsilon^3 \sqrt{2x}} \int_0^y \rho(x, \tilde{y}) d\tilde{y} \quad (10)$$

and are determined from the similarity equations given in Stewartson [16] and Ref. [14].

We begin by considering the flow in the vicinity of the leading edge where the streamwise length scale is $x = O(1)$. Since the inviscid velocity field can only depend on the streamwise coordinate through this relatively long streamwise length scale the solution for the velocity and temperature perturbation $\mathbf{u}' \equiv \{u', v', w', \vartheta'\}$ in this region is given by [14], [17]

$$\mathbf{u}' = \delta \left[u_\infty \{\bar{u}, \bar{v}, 0, \bar{\vartheta}\} + \bar{\beta}(\bar{w}_\infty + i\bar{v}_\infty) \left\{ \bar{u}^{(0)}, \bar{v}^{(0)}, \bar{w}^{(0)}, \bar{\vartheta}^{(0)} \right\} \right] e^{i(\bar{\beta}z/\varepsilon - t)}, \quad (11)$$

where $\left\{ \bar{u}^{(0)}(x, \eta), \bar{v}^{(0)}(x, \eta), \bar{w}^{(0)}(x, \eta), \bar{\vartheta}^{(0)}(x, \eta) \right\}$ satisfies the three dimensional compressible linearized boundary layer equations (with unit spanwise wavenumber) subject to the boundary conditions [14]

$$\bar{u}^{(0)}, \bar{\vartheta}^{(0)} \rightarrow 0, \quad \bar{w}^{(0)} \rightarrow e^{ix}, \quad \text{as } \eta \rightarrow \infty, \quad (12)$$

while $\{\bar{u}(x, \eta), \bar{v}(x, \eta), 0, \bar{\vartheta}(x, \eta)\} \exp i(\bar{\beta}z/\varepsilon - t)$ is a quasi-two dimensional solution that satisfies the two dimensional linearized boundary layer equations subject to the boundary conditions

$$\bar{u} \rightarrow e^{ix}, \quad \bar{w}, \bar{\vartheta} \rightarrow 0 \quad \text{as } \eta \rightarrow \infty. \quad (13)$$

The lowest order triple-deck solution will match onto the quasi-two dimensional solution $\{\bar{u}, \bar{v}, 0, \bar{\vartheta}\} \exp i(\bar{\beta}z/\varepsilon - t)$ of the two dimensional boundary layer equations, where the spanwise dependence only enters parametrically through the exponential factor in (11).

Prandtl [18], Glauert [19] and Lam and Rott [20] showed that

$$\bar{u}(x, \eta) = -\frac{B(x)U'(\eta)}{T\sqrt{2x}}, \quad \bar{\vartheta}(x, \eta) = -\frac{B(x)T'(\eta)}{T(\eta)\sqrt{2x}}, \quad (14)$$

$$\bar{v}(x, \eta) = iB(x) + \frac{dB}{dx}U(\eta) - B(x)\frac{U'(\eta)\eta_c}{2x}, \quad (15)$$

where

$$\eta_c \equiv \frac{1}{T(\eta)} \int_0^\eta T(\tilde{\eta}) d\tilde{\eta} \quad (16)$$

is an exact eigensolution of the two-dimensional linearized unsteady boundary layer equations that satisfies the homogeneous boundary conditions $\bar{u}(x, \eta), \bar{w}(x, \eta), \bar{\vartheta}(x, \eta) \rightarrow 0$ as $\eta \rightarrow \infty$ for all $B(x)$, but does not necessarily satisfy the no-slip condition at the wall.

Lam and Rott [20], [21] analyzed the two dimensional flat plate boundary layer and showed that the linearized equations possess asymptotic eigensolutions that satisfy a no-slip condition at the wall when x becomes large. These solutions exhibit a two-layer structure consisting of an outer region that encompasses the main part of the boundary layer and a thin viscous region near the wall. The outer solution is given by (14) and (15) with the arbitrary function $B(x)$ determined by matching with the viscous wall layer flow.

Ref. [14] showed that the Lam and Rott [20, 21] analysis also applies to compressible flows when the full compressible solution (14) and (15) is used in the outer region and the viscous wall layer solution is slightly modified to account for the temperature and viscosity variations. The function $B(x)$ is then given by

$$B(x) = x^{3/2} B_n \exp \left[-\frac{2^{3/2} e^{i\pi/4}}{3\lambda\zeta_n^{3/2}} \left(\frac{T_w}{\mu_w} \right)^{1/2} x^{3/2} \right] + \dots \quad (17)$$

where $T_w \equiv T(0)$, $\mu_w \equiv \mu(T(0))$, $\lambda \equiv U'(0)$ and ζ_n is a root of

$$Ai'(\zeta_n) = 0, \quad \text{for } n = 0, 1, 2, 3, \dots \quad (18)$$

The only difference from the Lam-Rott result is the $(T_w/\mu_w)^{1/2}$ factor in the exponent. The asymptotic solution to the full inhomogeneous boundary value problem can now be expressed as the sum of a Stokes layer solution plus a number of these asymptotic eigensolutions. The first few B_n were determined from

numerical solutions to the boundary layer problem in Ref. [8]. But we are primarily concerned with the lowest order $n = 0$ mode because that is the only one that matches onto a spatially growing oblique Tollmien-Schlichting wave further downstream [11]. The receptivity problem can then be solved by combining the numerical computations with appropriate matched asymptotic expansions to relate the instability wave amplitude to that of the free-stream disturbance. But we will analyze the boundary layer disturbances generated by the free-stream acoustic disturbances before considering these expansions.

3.2 Boundary layer disturbances generated by the Fedorov/Khokhlov mechanism for obliqueness angles close to critical angle

Fedorov and Khokhlov [10] used matched asymptotic expansions to analyze the generation of Mack mode instabilities by oblique acoustic waves of the form (4) where the wavenumbers α and β satisfy the dispersion relation (7) when the incidence angle γ is equal to zero, which, as noted, above is the case being considered here. Their focus was on hypersonic flows where the most rapidly growing disturbances are usually two dimensional 2nd Mack modes, while, as noted in the introduction, the focus of the present chapter is on the relatively low supersonic Mach number regime (say, less than about 4) where the most rapidly growing instability waves are highly oblique 1st Mack modes. Numerical results [9] show that the obliqueness angle of the most rapidly growing 1st mode lies between 50 and 70 degrees at Mach numbers between 2 and 6.

Ref. [10] shows that the boundary layer disturbance produced by diffraction of the slow acoustic wave by the nonparallel mean flow in the region where $x = o(\varepsilon^{-3})$ can be matched onto a 1st Mack mode instability in the downstream region where $x = O(\varepsilon^{-6})$ when the deviation

$$\Delta\theta \equiv \theta_c - \theta \quad (19)$$

of the obliqueness angle θ from the critical angle

$$\cos \theta_c \equiv 1/M_\infty \quad (20)$$

takes on $O(1)$ positive values. The diffraction region has a double layer structure which consists of a region that fills the mean boundary layer and an outer diffraction region of thickness $O(1/\varepsilon^{3/2})$. (The purely passive Stokes layer near the wall does not play a role in the diffraction process and can be ignored).

The instability emerges from the downstream limit of the solution in this region. But as noted in the introduction this occurs too far downstream to be of practical interest when scaled up to actual flight conditions if $\Delta\theta = O(1)$ [14] at the moderately supersonic Mach numbers being considered here. It will however emerge much further upstream when θ is close to the critical angle θ_c , i.e., when $\Delta\theta \ll 1$. But the solution in Ref. [10] does not apply when $\Delta\theta \ll 1$ and a new analysis was developed in Ref. [11] to extend their result into the small $-\Delta\theta$ regime.

It follows from (7) that

$$\alpha = \tilde{\alpha}/\Delta\theta + \tilde{\alpha}_1 + \dots, \quad \beta = \beta_1 = \tilde{\beta}/\Delta\theta \quad (21)$$

where

$$\tilde{\alpha} \equiv 1/\tan \theta_c, \tilde{\beta} \equiv 1, \tilde{\alpha}_1 \equiv 1/\sin^2 \theta_c \quad (22)$$

when $\Delta\theta \ll 1$ since $\tan(\theta_c - \Delta\theta) = \tan\theta_c - \Delta\theta/\cos^2\theta_c + O(\Delta\theta)^2$ in that case.

This shows that α also becomes large when $\Delta\theta \ll 1$ and that α will expand in powers of $\Delta\theta$ as indicated in (21) if β is fixed at the indicated value to all orders in $\Delta\theta$ (which we now assume to be the case).

The spanwise wavenumber will equal the vortical spanwise wavenumber (8) when $\Delta\theta = O(\varepsilon)$ and as in that case the diffraction wave solution will eventually develop a triple-deck structure but the resulting solution will (as shown in [11]) not decay at large wall normal distances and is therefore invalid. This means that the diffraction region solution cannot be continued downstream for $\Delta\theta = O(\varepsilon)$.

Ref. [11] shows that the smallest value of $\Delta\theta$ is $\Delta\theta = O(\varepsilon^{2/3})$ and the diffraction region will then occur at an $O(\varepsilon^{-4/3})$ distance downstream. The relevant solution will have the triple-deck structure shown in **Figure 3**: a main boundary layer region that fills the mean boundary layer (region 1), an outer diffraction region of thickness $O(\varepsilon^{-1/3})$ (region 2) and an $O(\varepsilon^3)$ thick viscous wall layer in which the unsteady, convective and viscous terms all balance.

The pressure in region 2 is of the form

$$p = 1 + \delta p_2(x_2, y_2) e^{i[(\tilde{\alpha}/\Delta\theta + \tilde{\alpha}_1)x + \tilde{\beta}z/\Delta\theta - t]}, \quad (23)$$

where

$$x_2 \equiv x\varepsilon^{4/3} = O(1), \quad y_2 \equiv y\varepsilon^{1/3} = O(1) \quad (24)$$

and the surface pressure $p_2(x_2, 0)$ is related to the up-wash velocity $v_1(x_2, \infty) \equiv \lim_{\eta \rightarrow \infty} v_1(x_2, \eta)$ at the outer edge of the boundary layer by

$$p_2(x_2, 0) = p_1(x_2) = 1 - \frac{x_2}{\sqrt{2\pi i \tilde{\alpha} (M_\infty^2 - 1)}} \int_0^1 \frac{\sqrt{\sigma}}{\sqrt{1 - \sigma}} i \tilde{\alpha} \left[\frac{v_1(x_2 \sigma, \infty)}{\sqrt{x_2 \sigma}} \right] d\sigma, \quad (25)$$

where $p_1(x_2)$ denotes the pressure in the boundary layer region 1 (which is independent of the wall normal direction) and the wall normal velocity $v_1(x_2, \infty)$ is given in terms of

$$\xi_2 \equiv -i^{1/3} \left(\sqrt{2x_2/\tilde{\alpha}\lambda} \right)^{2/3} (T_w/\mu_w)^{1/3} \quad (26)$$

and the integral and the derivative of the Airy function $Ai(\xi)$ by

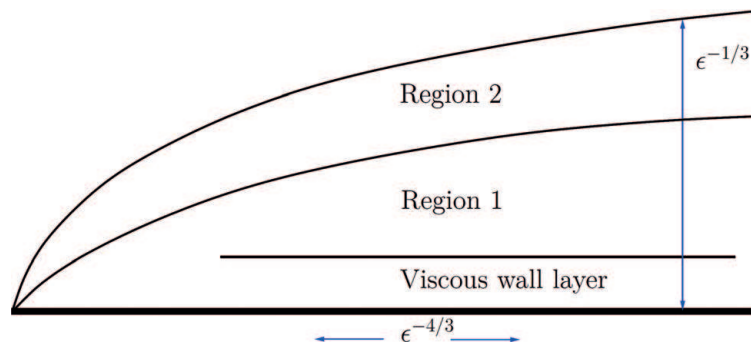


Figure 3.
Structure of diffraction region for $\Delta\theta = O(\varepsilon^{2/3})$.

$$\frac{v_1(x_2, \infty)}{\sqrt{2x_2}} = ip_1(x_2) \frac{(\tilde{\alpha}^2 + \tilde{\beta}^2) T_w^2 \xi_2}{\lambda Ai'(\xi_2)} \int_{\xi_2}^{\infty} Ai(\xi) d\xi, \quad (27)$$

which behaves like

$$v_1(x_2, \infty)/\sqrt{2x_2} \sim -ip_1(x_2) (\tilde{\alpha}^2 + \tilde{\beta}^2) T_w^2/\lambda \quad (28)$$

as $x_2 \rightarrow \infty$ since ([22], pp. 446–447)

$$Ai'(\xi)/\int_{\xi}^{\infty} Ai(q) dq \rightarrow -\xi \text{ as } \xi \rightarrow \infty. \quad (29)$$

Inserting (28) and (27) into (25) shows that

$$p_1(x_2) = 1 - \gamma_0 x_2 \int_0^1 \frac{\sqrt{\sigma}}{\sqrt{1-\sigma}} p_1(\sigma x_2) d\sigma, \text{ as } x_2 \rightarrow \infty \quad (30)$$

where

$$\gamma_0 \equiv \frac{(\tilde{\alpha}^2 + \tilde{\beta}^2) \tilde{\alpha}^{1/2} T_w^2}{\lambda \sqrt{2\pi i (M_{\infty}^2 - 1)}}, \quad (31)$$

which is formally the same as the equation considered in [10] who showed that the solution behaves like

$$p_1(x_2) \sim \exp \left[\gamma_0^2 \pi (x_2)^2 \right] \text{ as } x_2 \rightarrow \infty. \quad (32)$$

The acoustically and vortically generated boundary layer disturbances considered in this section will eventually evolve into propagating eigensolutions in regions that lie further downstream. The resulting flow will have a triple-deck structure of the type considered in [13], [23] and [14] in the former (i.e., vortically generated) case. But the acoustically generated disturbance will only develop an eigensolution structure much further downstream. The minimum distance occurs when $\Delta\theta = O(\epsilon^{2/3})$. We begin by considering the triple-deck region.

4. The viscous triple-deck region

Refs. [13, 14, 23] show that the linearized Navier-Stokes equations possess an eigensolution of the form

$$\{u, v, w, p\} = \hat{\delta} \Pi(y, \epsilon) e^{i \left[\frac{1}{\epsilon^2} \int_0^{x_1} \kappa(x_1, \epsilon) dx_1 + \bar{\beta} \bar{z} - t \right]} \quad (33)$$

in the triple-deck region where $\hat{\delta} \ll 1$ is the common scale factor introduced at the beginning of Section 2,

$$\Pi(y, \varepsilon) = \left\{ \frac{\bar{A}(x_1)U'(\eta)}{T(\eta)}, -i\kappa_0\bar{A}(x_1)U(\eta)\sqrt{2x_1}, -\frac{\varepsilon^2\bar{\beta}\bar{P}T(\eta)}{\kappa_0U(\eta)}, \varepsilon^2\bar{P} \right\} \quad (34)$$

in the main boundary layer where $\eta = O(1)$,

$$x_1 \equiv \varepsilon^2 x = O(1) \quad (35)$$

and

$$\bar{z} \equiv z/\varepsilon = z^* \omega^* / \varepsilon U_\infty^* \quad (36)$$

is a scaled transverse coordinate. The complex wavenumber κ has the expansion [11].

$$\kappa(x_1, \varepsilon) = \kappa_0(x_1) + \varepsilon\kappa_1(x_1) + \varepsilon^2\kappa_2(x_1) + \dots, \quad (37)$$

where the lowest order term in this expansion satisfies the following dispersion relation ([13, 14, 23])

$$\kappa_0^2 + \bar{\beta}^2 = \frac{1}{(i\kappa_0)^{1/3}} \left(\frac{\lambda}{\sqrt{2x_1}} \right)^{5/3} \left(\frac{\mu_w}{T_w} \right)^{1/3} \frac{[\bar{\beta}^2 - (M_\infty^2 - 1)\kappa_0^2]^{1/2} Ai'(\xi_0)}{\int_{\xi_0}^{\infty} Ai(q) dq} \quad (38)$$

and

$$\xi_0 = -i^{1/3} \left(\frac{\sqrt{2x_1}}{\kappa_0 \lambda} \right)^{2/3} (T_w/\mu_w)^{1/3} \quad (39)$$

whose solution must satisfy the inequality

$$\text{Re} [\bar{\beta}^2 - (M_\infty^2 - 1)\kappa_0^2]^{1/2} \geq 0 \quad (40)$$

in order to insure that the eigensolution does not exhibit unphysical wall normal growth.

This requirement will be satisfied for all $M_\infty < 1$ but will only be satisfied at supersonic Mach numbers when the obliqueness angle θ is greater than the critical angle $\theta_c \equiv \cos^{-1}(1/M_\infty)$ [11, 13]. The dispersion relation (38) and (39) reduces to the dispersion relation given by Eqs. (4.52), (5.2) and (5.3) of [7] when $\bar{\beta}$ and M_∞ are set to zero.

4.1 Matching with the Lam-Rott solution

The dispersion relation (38) and (39) will be satisfied at small values of x_1 if $\kappa_0 \sim \sqrt{x_1}$ and $\xi_0 \rightarrow \zeta_n$, for $n = 0, 1, 2, \dots$ as $x_1 \rightarrow 0$, where ζ_n is the n th root of the Lam-Rott dispersion relation (18). Inserting this into (38) shows that

$$\kappa_0 \rightarrow \frac{1}{\lambda \zeta_n^{3/2}} \left(\frac{2T_w x_1}{i\mu_w} \right)^{1/2} \text{ as } x_1 \rightarrow 0. \quad (41)$$

The cross flow velocity w drops out of (33) as $x_1 \rightarrow 0$ and the flow in the main deck is therefore compatible with the quasi-two dimensional Lam-Rott solution (14)–(17).

4.2 Numerical results

The dispersion relation (38) is expected to have at least one root corresponding to each of the infinitely many roots of (18). But only the lowest order $n = 0$ root can produce the spatially growing modes of (38). The wall temperature T_w and viscosity μ_w can be scaled out of this equation by introducing the rescaled variables.

$$\kappa_0^\dagger = \kappa_0 T_w^{1/2} \mu_w^{1/6}, x_1^\dagger = x_1 T_w^2 / \mu_w^{2/3}, \bar{\beta}^\dagger = \bar{\beta} T_w^{1/2} \mu_w^{1/6}. \quad (42)$$

The real and negative imaginary parts of κ_0^\dagger calculated from (38) together with the $n = 0$ Lam-Rott initial condition (41) are plotted as a function of the scaled streamwise coordinate \bar{x}_1^\dagger in **Figures 4** and **5** for three values of the frequency scaled transverse wavenumber $\bar{\beta}^\dagger \geq 2$. The insets are included to more clearly show the changes at small \bar{x}_1^\dagger . The dashed curves in the insets denote the real and imaginary parts of the small- \bar{x}_1^\dagger asymptotic formula (41).

The triple-deck eigensolution (33) (which contains the Lam-Rott solution as an upstream limit) can undergo a significant amount of damping before it turns into a spatially growing instability wave at the lower branch of the neutral stability curve.

The exponential damping in Eq. (33) is proportional to $\gamma_m \int_0^{x_{LB}} \kappa(x_1) dx = \varepsilon^{-2} \gamma_m \int_0^{(x_1)_{LB}} \kappa(x_1) dx_1$, where $(x_1)_{LB}$ and x_{LB} denote the scaled and unscaled streamwise location of the lower branch of the neutral stability, which implies that the total damping is proportional to the area under the growth rate curve between zero and the lower branch in **Figure 5**. The inset shows that the length $\Delta x_1^\dagger = 0.01$ of this upstream region is very short and therefore that the total amount of damping is relatively small.

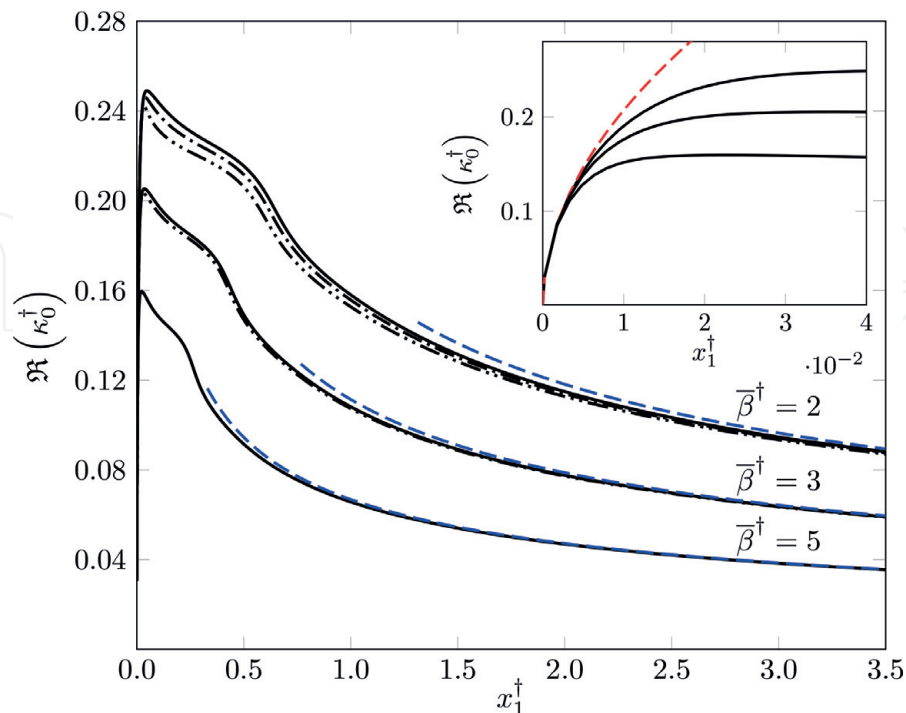


Figure 4. $\Re(\kappa_0^\dagger)$ as a function of x_1^\dagger calculated from (38) together with the initial condition (41) for $M_\infty = 2, 3, 4$ (double dot dashed, dot dashed, and solid lines, respectively) and three values of $\bar{\beta}^\dagger \geq 2$. The dashed curve in the main graph is the rescaled large- x_1^\dagger asymptote (49).

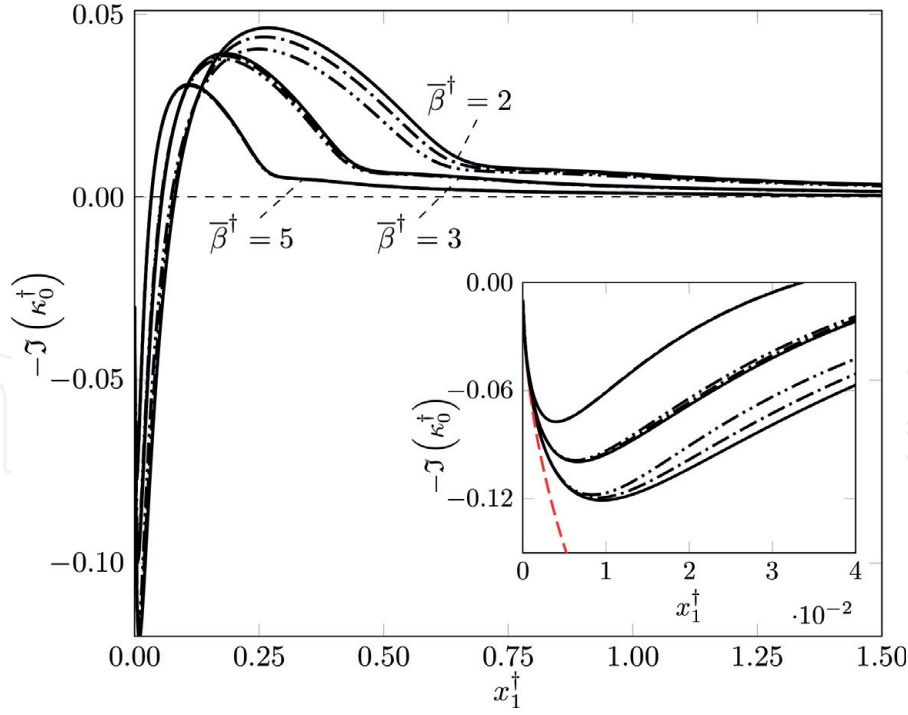


Figure 5. $-\text{Im}(\kappa_0^\dagger)$ as a function of x_1^\dagger calculated from (38) together with the initial condition (41) for $M_\infty = 2, 3, 4$ (double dot dashed, dot dashed and solid lines, respectively) and three values of the frequency scaled transverse wavenumber.

5. The inviscid triple-deck region

As noted above the acoustically driven solution will only match onto an eigensolution in the downstream region when $O(\Delta\theta) \geq \varepsilon^{3/2}$. This region will lie downstream of the viscous triple-deck region considered above and will be closest to that region when $O(\Delta\theta) = \varepsilon^{3/2}$. It will have an inviscid triple-deck structure and the relevant dispersion relation can be obtained by putting $\varepsilon/\Delta\theta = O(\varepsilon^{1/3})$ in (21), inserting the rescaled variables

$$\bar{\bar{\beta}} = \bar{\beta}/\varepsilon^{1/3}, \bar{\bar{\kappa}}_0 = \kappa_0/\varepsilon^{1/3}, \hat{x}_1 = x_1\varepsilon^{4/3} \quad (43)$$

into (38), using (29), and taking the limit as $\varepsilon \rightarrow 0$ with $\bar{\bar{\beta}}$, $\bar{\bar{\kappa}}_0$ and \hat{x}_1 held fixed, to show that the rescaled wavenumber $\bar{\bar{\kappa}}_0$ satisfies the inviscid dispersion relation

$$\bar{\bar{\kappa}}_0^2 + \bar{\bar{\beta}}^2 = \frac{\lambda \left[\bar{\bar{\beta}}^2 - (M_\infty^2 - 1)\bar{\bar{\kappa}}_0^2 \right]^{1/2}}{\bar{\bar{\kappa}}_0 \sqrt{2\hat{x}_1} T_w^2} \quad (44)$$

when the square root $\left[\bar{\bar{\beta}}^2 - (M_\infty^2 - 1)\bar{\bar{\kappa}}_0^2 \right]^{1/2}$ is required to remain finite as $\varepsilon \rightarrow 0$.

5.1 Matching with the small $\Delta\theta$ Fedorov/Khokhlov solution

It can then be shown by direct substitution that the solution $\bar{\bar{\kappa}}_0$ behaves like

$$\bar{\bar{\kappa}}_0 \rightarrow \frac{\bar{\bar{\beta}}}{(M_\infty^2 - 1)^{1/2}} - \bar{\bar{\beta}}^5 \hat{\alpha}_0^2 \hat{x}_1 \quad \text{as } \hat{x}_1 \rightarrow 0, \quad (45)$$

where $\hat{\alpha}_0 \equiv M_\infty^2 T_w^2 / [(M_\infty^2 - 1)^{7/4} \lambda]$. The square root $\left[\bar{\beta}^2 - (M_\infty^2 - 1) \bar{\kappa}_0^2 \right]^{1/2}$ still satisfies the inequality (40) when $\hat{x}_1 \rightarrow 0$ and (44) therefore remains valid in this limit.

The pressure component of the resulting solution will then match onto the downstream limit (32) and (30) of the acoustically generated diffraction region solution when $\bar{\beta} = O(\epsilon^{2/3} / \Delta\theta)$ and x_2 is given by (24) since it follows from (8), (35), (43) and (45) that

$$\begin{aligned} (1/\epsilon^3) \int_0^{x_1} \kappa_0(x_1) dx_1 &= (1/\epsilon^4) \int_0^{\hat{x}_1} \bar{\kappa}_0(\hat{x}_1) d\hat{x}_1 \rightarrow (\tilde{\alpha}/\Delta\theta)x - \epsilon \bar{\beta}^5 \hat{\alpha}_0^2 x^2/2 \\ &= (\tilde{\alpha}/\Delta\theta)x - \beta^5 \hat{\alpha}_0^2 (\epsilon^3 x)^2/2 = (\tilde{\alpha}/\Delta\theta)x - \hat{\alpha}_0^2 x_2^2/2. \end{aligned} \tag{46}$$

5.2 Numerical results

Figure 6 is a plot of the scaled lowest order wavenumber $\bar{\kappa}_0/\bar{\beta} = \kappa_0/\bar{\beta}$ as a function of the scaled streamwise coordinate $(\bar{\beta}T_w)^4 \hat{x}_1/\lambda^2 = (\bar{\beta}T_w)^4 x_1/\lambda^2$ for various values of the free-stream Mach number M_∞ calculated from the inviscid triple-deck dispersion relation (44) together with the asymptotic initial condition (45) which is shown by the dashed curves in the figure. The lowest order wave number $\bar{\kappa}_0$ is purely real which means that exponential growth (if it occurs) can only occur at higher order. This suggests that the acoustically generated instabilities will be less significant than the vortically-generated instabilities which appear upstream.

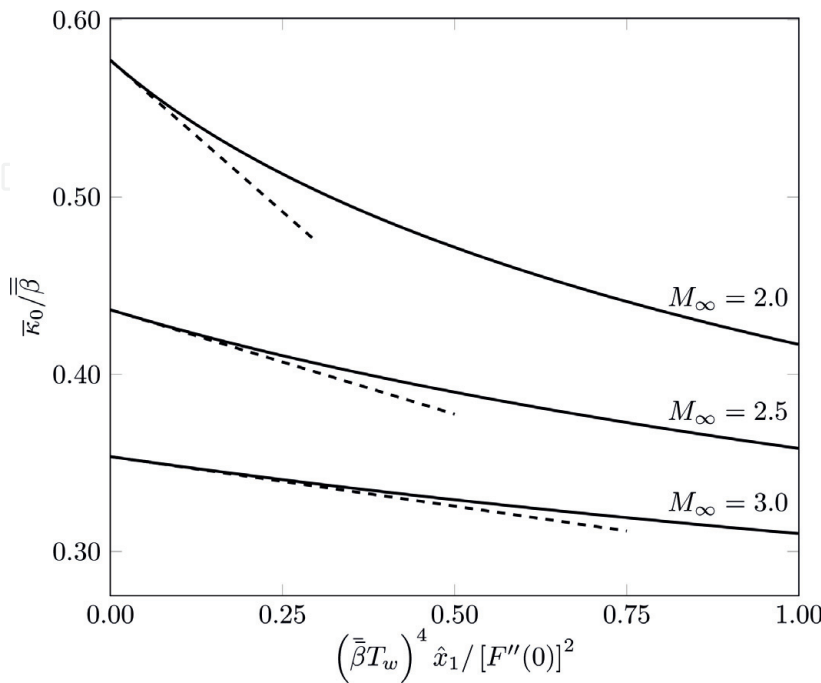


Figure 6. Scaled wavenumber $\bar{\kappa}_0/\bar{\beta} = \kappa_0/\bar{\beta}$ as a function of $(\bar{\beta}T_w)^4 \hat{x}_1/\lambda^2 = (\bar{\beta}T_w)^4 x_1/\lambda^2$ for various values of M_∞ . The solid lines represent the numerical solution. Dashed lines are the asymptotic solution (45).

6. The next stage of evolution

6.1 Downstream behavior of the triple-deck solution

Eqs. (29), (38) and (39) show that

$$\bar{\beta} \rightarrow \frac{1}{\kappa_0^{1/3}} \left(\frac{\lambda}{\sqrt{2x_1}} \right)^{5/3} \left(\frac{1}{T_w^2} \right) \left(\frac{\sqrt{2x_1}}{\kappa_0 \lambda} \right)^{2/3} = \frac{\lambda}{\kappa_0 T_w^2 \sqrt{2x_1}} \quad (47)$$

when $x_1 \rightarrow \infty$ and, therefore, that

$$\kappa_0 \rightarrow \frac{\lambda}{\bar{\beta} T_w^2 \sqrt{2x_1}}, \quad (48)$$

when κ_0 is allowed to approach zero as $x_1 \rightarrow \infty$.

The dashed curves in the main plot of **Figure 4** represent the re-scaled large- \bar{x}_1^\dagger asymptote (48). It confirms that the numerical results are well approximated by the (appropriately rescaled) large- x_1 asymptote (48).

As noted in [11], the solution to the reduced dispersion relation (44) satisfies the rescaled version

$$\bar{\kappa}_0 \rightarrow \frac{\lambda}{\bar{\beta} T_w^2 \sqrt{2\hat{x}_1}} \text{ as } \hat{x}_1 \rightarrow \infty \quad (49)$$

of (48), which can be considered to be a special case of this result if we put

$$\bar{\beta} = \bar{\beta}/\varepsilon^r, \bar{\kappa}_0 = \kappa_0/\varepsilon^r, \hat{x}_1 = x_1 \varepsilon^{4r} \quad (50)$$

and allow r to be zero or $1/3$.

The expansion (37) then generalizes to [11]

$$\bar{\kappa}(x_1, \varepsilon) = \bar{\kappa}_0(\hat{x}_1) + \varepsilon^{1-r} \bar{\kappa}_1(\hat{x}_1) + \varepsilon^{2(1-r)} \bar{\kappa}_2(\hat{x}_1) + \dots, \quad (51)$$

where

$$\bar{\kappa}, \bar{\kappa}_1, \bar{\kappa}_2 \dots \equiv \kappa/\varepsilon^r, \kappa_1, \kappa_2 \varepsilon^r \dots \quad (52)$$

and \hat{x}_1 is defined in (43).

6.2 Derivation of the governing equations

Eq. (49) shows, among other things, that the lowest order wave number and streamwise growth rate approach zero but do not become negative as the disturbance propagates downstream. The boundary layer thickness which is $O(\varepsilon^3 \sqrt{x})$ continues to increase and the triple-deck scaling breaks down at the streamwise location

$$\bar{x}_1 = x \varepsilon^{4+2r} = O(1), \quad (53)$$

where it becomes of the order of the spanwise length scale, which remains constant at $O(\varepsilon^{1-r})$. This region is located well upstream of the region where the unsteady flow is governed by the full Rayleigh equation considered in [9].

Eqs. (37), (43), (51) and (52) show that the Tollmien-Schlichting wave becomes more oblique and

$$\exp i \left[\frac{1}{\varepsilon^3} \int_0^{\hat{x}_1} \kappa(\hat{x}_1, \varepsilon) d\hat{x}_1 + \bar{\beta} \bar{z} - t \right] = \exp i \left[\frac{1}{\varepsilon^{3(1+r)}} \int_0^{\hat{x}_1} \bar{\kappa}_0(\hat{x}_1, \varepsilon) d\hat{x}_1 + \frac{1}{\varepsilon^{2+4r}} \int_0^{\hat{x}_1} \bar{\kappa}_1(\hat{x}_1, \varepsilon) d\hat{x}_1 \right. \\ \left. + \frac{1}{\varepsilon^{1+5r}} \int_0^{\hat{x}_1} \bar{\kappa}_2(\hat{x}_1, \varepsilon) d\hat{x}_1 + O(\varepsilon^{-4r}) + \varepsilon^r \bar{\beta} \bar{z} - t \right] \rightarrow e^{i \left[\frac{1}{\varepsilon^{-2(2+r)}} \int_0^{\bar{x}_1} \bar{\alpha}(\bar{x}_1, \varepsilon) d\bar{x}_1 + \bar{\beta} \bar{z} - t \right]} \quad (54)$$

as $\hat{x}_1 \rightarrow \infty$, where $\bar{\alpha}(\bar{x}_1)$ is an $O(1)$ function of \bar{x}_1 (given by (53)) and

$$\bar{z} \equiv \varepsilon^r \bar{z} = z / \varepsilon^{1-r}, \quad (55)$$

which means that the solution should be proportional to

$$\exp i \left[\varepsilon^{-(4+2r)} \int_0^{\bar{x}_1} \bar{\alpha}(\bar{x}_1, \varepsilon) d\bar{x}_1 + \bar{\beta} \bar{z} - t \right], \text{ where } \bar{\alpha}(\bar{x}_1) \text{ is an } O(1) \text{ function of } \bar{x}_1 \text{ that}$$

behaves like

$$\bar{\alpha} \rightarrow \frac{\lambda}{\bar{\beta} T_w^2 \sqrt{2\bar{x}_1}} + \dots \text{ as } \bar{x}_1 \rightarrow 0 \quad (56)$$

in this stage of evolution. The solution should remain inviscid in the main boundary layer and the viscous wall layer (i.e., a Stokes layer) is expected to be completely passive.

The scaled variable

$$\bar{y} \equiv y / \varepsilon^{1-r} \quad (57)$$

will be $O(1)$ in the main boundary layer since its thickness is now of the order of the spanwise length scale, $O(\varepsilon^{1-r})$. It therefore follows from (53) and (57) that the transverse pressure gradients will come into play and the solution in this region should expand like

$$\{u, v, w, p\} = \{U, 0, 0, 0\} + \hat{\delta} \mathcal{A}(\bar{x}_1) \{ \bar{u}(\bar{y}; \bar{x}_1), \varepsilon^{1-r} \bar{v}(\bar{y}; \bar{x}_1), \varepsilon^{1-r} \bar{w}(\bar{y}; \bar{x}_1), \varepsilon^{2(1-r)} \bar{p}(\bar{y}; \bar{x}_1) \}$$

$$\exp i \left[\frac{1}{\varepsilon^{4+2r}} \int_0^{\bar{x}_1} \bar{\alpha}(\bar{x}_1, \varepsilon) d\bar{x}_1 + \bar{\beta} \bar{z} - t \right] \dots \quad (58)$$

where $\mathcal{A}(\bar{x}_1)$ is a function of the slow variable \bar{x}_1 . Substituting (58) into the linearized Navier-Stokes equations shows that the wall normal velocity perturbation \bar{v} is determined by the incompressible reduced Rayleigh equation

$$T \frac{d}{d\bar{y}} \frac{1}{T} \frac{d\bar{v}}{d\bar{y}} + \left[\frac{T\bar{\alpha}}{1 - \bar{\alpha}U} \frac{d}{d\bar{y}} \left(\frac{dU/d\bar{y}}{T} \right) - \bar{\beta}^2 \right] \bar{v} = 0 \quad (59)$$

whose solution must satisfy the following boundary conditions

$$\bar{v} \sim e^{-\bar{\beta}\bar{y}} \text{ as } \bar{y} \rightarrow \infty, \quad \bar{v} = 0 \text{ at } \bar{y} = 0. \quad (60)$$

Matching with the upstream solution (33) and (37) requires that $\bar{\alpha}(\bar{x}_1)$ satisfy the matching condition (56) as $\bar{x}_1 \rightarrow 0$.

Inserting (10) and (57) into (59), using (60) and assuming the ideal gas law $\rho T = 1$ shows that

$$\frac{d}{d\eta} \frac{1}{T^2} \frac{d\bar{v}}{d\eta} + \left[\frac{\bar{\alpha}}{1 - \bar{\alpha}U} \left(\frac{U'}{T^2} \right)' - \left(\bar{\beta} \sqrt{2\bar{x}_1} \right)^2 \right] \bar{v} = O\left(\varepsilon^{2(1-r)}\right), \quad (61)$$

$$\bar{v} = 0 \text{ at } \eta = 0, \quad (62)$$

which means that

$$\bar{\alpha} = f(\hat{\beta}), \quad (63)$$

where

$$\hat{\beta} \equiv \bar{\beta} \sqrt{2\bar{x}_1}. \quad (64)$$

6.3 Matching with the triple-deck solution

Eq. (64) clearly approaches zero when $\bar{x}_1 \rightarrow 0$, which means that $\bar{\alpha}$ will be consistent with the matching condition (54) if we require that it behave like

$$\bar{\alpha} = \lambda/T_w^2 \hat{\beta} + \alpha_1 + \alpha_2 \hat{\beta} + \dots \text{ as } \bar{x}_1 \rightarrow 0 \quad (65)$$

where $\alpha_1, \alpha_2, \dots$ are (in general complex) constants such that

$$\alpha_1 = \lim_{\hat{x}_1 \rightarrow \infty} \bar{\kappa}_1(\hat{x}_1), \alpha_2 = \lim_{\hat{x}_1 \rightarrow \infty} \bar{\kappa}_2(\hat{x}_1)/\bar{\beta} \sqrt{2\hat{x}_1}. \quad (66)$$

Ref. [11] proved that (60)–(64) possess an asymptotic solution of the form $\bar{v} = U(\eta) + \hat{\beta}v_1 + \hat{\beta}^2v_2 + \dots$ as $\hat{\beta} \rightarrow 0$ when $\bar{\alpha}$ satisfies (65) which implies that their solutions are able to match onto the lowest order triple-deck solution upstream and are consistent with the higher order solutions in this region.

6.4 Numerical results

The Rayleigh eigenvalues $\bar{\alpha}$ are determined by the boundary value problem (60), (61) and (62). We assume in the following that the Prandtl number is equal to unity and that the viscosity $\mu(T)$ satisfies the simple linear relation $\mu(T) = T(\eta)$.

Parts (a) and (b) of **Figure 7** are plots of the real and imaginary parts respectively of these eigenvalues as a function of $\hat{\beta}$. They show that the numerical solution for $\bar{\alpha}$ will be consistent with the matching conditions (65) and (66) if the higher order terms in the triple-deck expansion (51) satisfy $\lim_{\hat{x}_1 \rightarrow \infty} \bar{\kappa}_1(\hat{x}_1) = 0$ and $\lim_{\hat{x}_1 \rightarrow \infty} \bar{\kappa}_2(\hat{x}_1)/\bar{\beta} \sqrt{2\hat{x}_1} = \pm iC$, where the values of C are given in the caption of **Figure 7**. They also show that $\bar{\alpha}$ is initially real and eventually becomes complex. But these eigenvalues must occur in complex conjugate pairs since the coefficients in (61) are all real. The computations show that $\Im(\bar{\alpha})$ eventually goes to zero at

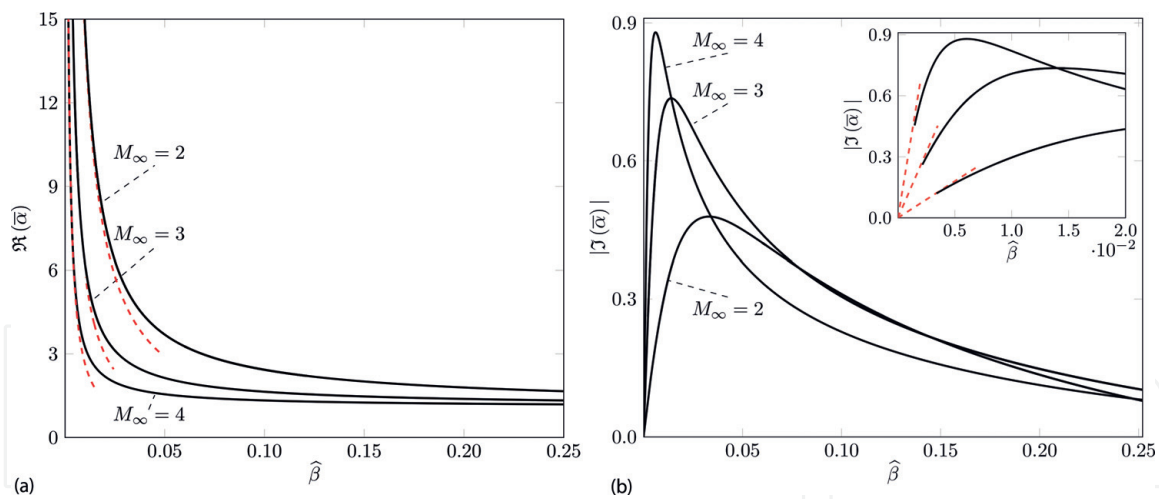


Figure 7.
 (a) $\Re(\bar{\alpha})$ and (b) $|\gamma_m(\bar{\alpha})|$ vs. $\hat{\beta}$ calculated from the modified Rayleigh solution. The red dashed curves are calculated from the asymptotic formula (56). The red dashed lines in the inset are $|\gamma_m(\bar{\alpha})| = C\hat{\beta}$, where $C = 36$ for $M_\infty = 2$, $C = 129.4$ for $M_\infty = 3$ and $C = 340.1$ for $M_\infty = 4$.

some finite value of $\hat{\beta}$ which is consistent with the fact that $(U'/T^2)'$ is equal to zero at some finite value of η and Eq. (61) therefore has a generalized inflection point there.

7. Conclusions

This chapter uses high Reynolds number asymptotics to study the nonlocal behavior of boundary layer instabilities generated by small amplitude free-stream disturbances at subsonic and moderate supersonic Mach numbers. The appropriate small expansion parameter turns out to be $\varepsilon = \mathcal{T}^{1/6}$, where \mathcal{T} denotes the frequency parameter. The oblique 1st Mack mode instabilities generated by free-stream acoustic disturbances are compared with those generated by elongated vortical disturbances. The focus is on explaining the relevant physics and not on obtaining accurate numerical predictions.

The free-stream vortical disturbances generate unsteady flows in the leading edge region that produce short spanwise wavelength instabilities in a viscous triple-deck region which lies at an $O(\varepsilon^{-2})$ distance downstream from the leading edge. The mechanism was first considered for two dimensional incompressible flows in Ref. [7], but the instability onset occurs much further upstream in the supersonic case and is, therefore, much more likely to be important at the higher Mach numbers considered in this chapter. The lowest order triple-deck solution does not possess an upper branch and evolves into an inviscid 1st Mack mode instability with short spanwise wavelength at an $O(\varepsilon^{-4})$ distance downstream.

Fedorov and Khokhlov [10] used asymptotic methods to study the generation of inviscid instabilities in supersonic boundary layers by fast and slow acoustic disturbances in the free stream whose obliqueness angle θ deviated from its critical value by an $O(1)$ amount and showed that slow acoustic disturbances generate unsteady boundary layer disturbances that produce $O(1)$ spanwise wavelength inviscid 1st Mack mode instabilities a much larger $O(\varepsilon^{-6})$ distance downstream. But the calculations in Ref. [11] show that the physical streamwise distance $x^* = (U_\infty^*)^3/(\omega^*)^2\nu_\infty^*$ corresponding to this scaled downstream location is at least equal to about 7 m for the typical supersonic flight conditions at

$M_\infty = 3$ ($U_\infty^* = 888 \text{ m/s}$, $\nu_\infty^* = 0.000264 \text{ m}^2/\text{s}$) end an altitude of 20 km with an upper bound of 100 kHz for the characteristic frequency. This means that this instability occurs too far downstream to be of any practical interest at the moderately low supersonic Mach numbers considered in this chapter.

But, the inviscid instability, which first appears at an $O(\varepsilon^{-(4+2/3)})$ distance downstream when $\Delta\theta$ is reduced to $O(\varepsilon^{2/3})$ can be significant when scaled to flight conditions. It is therefore appropriate to compare the vortically-generated instabilities with the instabilities generated by oblique acoustic disturbances with obliqueness angles in this range as done in this chapter.

Acknowledgements

This research was sponsored by NASA's by the Transformative Aeronautics Concepts Program of the Aeronautics Research Mission Directorate under the Transformational Tools and Technologies (TTT) Project. PR was supported by the Air Force Office of Scientific Research award number AFOSR Grant FA9550-15-1-0248. We would also like to thank Dr. Meelan Choudhari for bringing the photograph in **Figure 2** to our attention.

Author details


Marvin E. Goldstein^{1*} and Pierre Ricco²

¹ National Aeronautics and Space Administration, Glenn Research Centre, Cleveland, OH, USA

² Department of Mechanical Engineering, The University of Sheffield, Sheffield, UK

*Address all correspondence to: marvin.e.goldstein@nasa.gov

IntechOpen

© 2019 The Author(s). Licensee IntechOpen. This chapter is distributed under the terms of the Creative Commons Attribution License (<http://creativecommons.org/licenses/by/3.0>), which permits unrestricted use, distribution, and reproduction in any medium, provided the original work is properly cited. 

References

- [1] Dryden HL. Air flow in the boundary layer near a plate. NACA Report no. 562; 1936. Available from: <https://naca.central.cranfield.ac.uk/reports/1937/naca-report-562.pdf>
- [2] Marensi E, Ricco P, Wu X. Nonlinear unsteady streaks engendered by the interaction of free-stream vorticity with a compressible boundary layer. *Journal of Fluid Mechanics*. 2017;**817**:80-121
- [3] Reshotko E. Boundary layer stability and control. *Annual Review of Fluid Mechanics*. 1976;**8**:311-349
- [4] Goldstein ME. Scattering of acoustic waves into Tollmien-Schlichting waves by small streamwise variations in surface geometry. *Journal of Fluid Mechanics*. 1985;**154**:509-531
- [5] Ruban AI. On the generation of Tollmien-Schlichting waves by sound. *Fluid Dynamics*. 1985;**19**:709-716
- [6] Choudhari M, Street CL. Theoretical prediction of boundary-layer receptivity. In: AIAA paper 94-2223, 25th Fluid Dynamics Conference, Colorado Springs, CO; 1994
- [7] Goldstein ME. The evolution of Tollmien-Schlichting waves near a leading edge. *Journal of Fluid Mechanics*. 1983;**127**:59-81
- [8] Goldstein ME, Sockol PM, Sanz J. The evolution of Tollmien-Schlichting waves near a leading edge. Part 2. Numerical determination of amplitudes. *Journal of Fluid Mechanics*. 1983;**129**:443-453
- [9] Mack LM. Boundary layer linear stability theory. AGARD Report 709; 1984
- [10] Fedorov AV, Khokhlov AP. Excitation of unstable disturbances in a supersonic boundary layer by acoustic waves. *Fluid Dynamics*. 1991;**9**:457-467
- [11] Goldstein ME, Ricco P. Non-localized boundary layer instabilities resulting from leading edge receptivity at moderate supersonic Mach numbers. *Journal of Fluid Mechanics*. 2018;**838**:435-477. DOI: 10.1017/jfm2017.889
- [12] Fedorov AV. Receptivity of a high speed boundary layer to acoustic disturbances. *Journal of Fluid Mechanics*. 2003;**491**:101-129
- [13] Smith FK. On the first-mode instability in subsonic, supersonic or hypersonic boundary layers. *Journal of Fluid Mechanics*. 1989;**198**:127-153
- [14] Ricco P, Wu X. Response of a compressible laminar boundary layer to free-stream vortical disturbance. *Journal of Fluid Mechanics*. 2007;**587**:97-138. DOI: 10.1017/s0022112007007070
- [15] Kovasznay LSG. Turbulence in supersonic flow. *Journal of Aerosol Science*. 1953;**20**(10):657-674
- [16] Stewartson K. *The Theory of Laminar Boundary Layers in Compressible Fluids*. Clarendon Press; 1964
- [17] Gulyaev AN, Kozlov VE, Kuznetsov VR, Mineev BI, Sekundov AN. Interaction of a laminar boundary layer with external turbulence. *Izvestiya Akademii Nauk SSSR, Mekhanika Zhidkosti i Gaza* 1989;**6**:700-710
- [18] Prandtl L. Zur Berechnung der Grenzschichten. *Zeitschrift fuer Angewandte Mathematik und Mechanik*. 1938;**18**:77-82
- [19] Glauert MB. The laminar boundary layer on oscillating plates and cylinders.

Journal of Fluid Mechanics. 1956;**1**(1):
97-110

[20] Lam SH, Rott. Theory of Linearized
Time-Dependent Boundary Layers.
Ithaca, NY: Graduate School of
Aeronautical Engineering Report
AFSOR TN-60-1100, Cornell
University; 1960

[21] Lam SH, Rott. Eigen-functions of
unsteady boundary layer equations.
Journal of Fluid Engineering. 1995;
1995:115

[22] Abramowitz M, Stegun IA.
Handbook of Mathematical Functions.
Washington: National Bureau of
Standards; 1965

[23] Wu X. Generation of Tollmein-
Schlichting waves by convecting gusts
interacting with sound. Journal of Fluid
Mechanics. 1999;**397**:285-316